LAWRENCE
LIVERMORE
NATIONAL
LABORATORY

LLNL-JRNL-410491

DENSITY-FUNCTIONAL STUDY OF Zr-BASED ACTINIDE ALLOYS: 2. U-Pu-Zr SYSTEM

A. Landa, P. Soderlind, P. Turchi, L. Vitos, A. Ruban

February 11, 2009

Journal of Nuclear Materials

Disclaimer

Density-functional study of Zr-based actinide alloys: 2. U-Pu-Zr system

A. Landa[1*], P. Söderlind[1], P. E.A. Turchi[1], L. Vitos[2], and A. Ruban[2]

[1]Lawrence Livermore National Laboratory, Livermore, CA 94551, USA

[2]Royal Institute of Technology, SE-10044, Stockholm, Sweden

Abstract

Density-functional theory, previously used to describe phase equilibria in the U-Zr alloys [1], is applied to study ground state properties of the bcc U-Pu-Zr solid solutions. Calculated heats of formation of the Pu-U and Pu-Zr alloys are in a good agreement with CALPHAD assessments. We found that account for spin-orbit coupling is important for successful description of Pu-containing alloys.

Keywords: nuclear reactor materials, phase transitions, first principles.

[*] Corresponding author. Tel.: + 1 925 424 3523; fax: +1 925 422 2851. E-Mail address: landa1@llnl.gov

1. Introduction

In our previous paper, Ref. [1], we performed a detailed *ab initio* study of the main thermodynamic properties of the U-Zr alloy system that is a good nuclear fuel candidate for fast breeder reactors. Because the thermal conductivity of U-Zr alloys is one of the highest among nuclear fuels, the radial temperature gradient generated in fast breeder reactors appears to be sufficiently large to cause redistribution of the alloy constituents [2, 3]. The constituent redistribution alters alloy composition during irradiation, which affects local power production, variation in fission product generation, and irradiation behavior such as fuel swelling and growth.

Although the U-Zr alloys can be used as nuclear fuel, a fast rectors operation on a closed fuel cycle will, due to the nuclear reactions, contain significant amount of plutonium [3]. The ternary U-Pu-Zr phase diagram is very complex, although the constituent redistribution in the specific U-19Pu-10Zr (wt. %), or $U_{61}Pu_{16}Zr_{23}$ (at. %), alloy was studied in numerous publications [2-6]. This alloy is known to form: (i) a bcc solid solution (γ-phase) in the temperature range of 650-750 °C; (ii) a mixture of γ- and cubic ζ- phases in the temperature range of 600-650 °C; and (iii) below 600 °C the γ-phase transforms to the fcc δ-phase and a mixture of δ- and ζ–phase that exists in the temperature range of 500-600 °C [4, 5]. A detailed study of the microstructure of the irradiated U-19Pu-10Zr (wt. %) alloy [4-6] revealed three distinct concentric zones: the pure γ-phase Zr-enriched porous central zone, the Zr-depleted intermediate zone (γ + ζ mixture), and a slightly Zr-enriched zone on the periphery (δ +ζ mixture). Although Pu concentration remains almost constant in all three zones with a slight decrease toward the fuel surface, it is believed that Pu presence in the alloy at levels greater than 8 wt. %

enhances U and Zr migration [3, 5]. Even though both irradiated U-Zr and U-Pu-Zr alloys develop a porous Zr-enriched central and apparently dense Zr-depleted intermediate zone, a key difference exists in their microstructure [3]. In the irradiated U-Pu-Zr fuel the intermediate zone is almost completely depleted of Zr that migrates both radially inward (to the central zone) and outward (to the periphery). In contrast, evidence of outward Zr migration has not been found yet in the irradiated binary U-Zr fuel: the depleted intermediate zone retains a fair amount of Zr, and the amount of Zr lost from the depleted intermediate zone balances the amount gained in the enriched center [3]. The complex nature of constituent redistribution in the U-Pu-Zr alloys during irradiation and its influence on nuclear fuel performance makes study of this phenomenon extremely important.

Recent semi-empirical model calculations [2], supported by experimental observation, indicated that the excess enthalpy of solution of the bcc γ-U-Zr phase controls the constituent redistribution process. In our previous paper [1], we performed detailed calculations of the heat of formation of γ-U-Zr solid solutions. In this work we present results of similar calculations for γ-Pu-U and γ-Pu-Zr alloys that can be used for further analysis of the constituent redistribution in the central zone of U-Pu-Zr nuclear fuels.

In our calculations we employ three complementary computational techniques: (i) scalar-relativistic (SR) Green's function technique based on the Korringa-Kohn-Rostoker (KKR) method within the atomic-sphere approximation (ASA), (ii) scalar-relativistic and fully-relativistic (FR) exact muffin-tin orbital methods (EMTO), and (iii) the all-electron full-potential linear muffin-tin orbital method (FPLMTO) that also accounts for all

relativistic effects. Pertinent details of the computational methods are described in Section 2. Results of the density-functional calculations of the ground-state properties of the γ-Pu-U and γ-Pu-Zr solid solutions are presented in Section 3. Lastly, concluding remarks are presented in Section 4.

2. Computational details

The calculations we have referred to as KKR-ASA are performed using the SR Green's function technique based on the KKR method within the ASA [7-10]. For the present study this approximation is improved by including higher multipoles of the charge density [9] and the so-called muffin-tin correction [10] to the electrostatic energy. The calculations are performed for a basis set including valence *spdf* orbitals. For the electron exchange and correlation energy functional, the generalized gradient approximation (GGA) is considered [11]. Integration over the Brillouin zone is performed using the special *k*-point technique [12] with 506 points in the irreducible wedge of the zone for the bcc structure. The moment of the density of states, needed for the kinetic energy and valence charge density, are calculated by integrating the Green's function over a complex energy contour (with a 2.5 Ry diameter) using a Gaussian integration technique with 30 points on a semi-circle enclosing the occupied states. The equilibrium density of the U-Zr, Pu-U, and Pu-Zr alloys is obtained from a Murnaghan [13] fit to the total energy versus lattice constant curve.

In order to treat compositional disorder the KKR-ASA method is combined with the coherent potential approximation (CPA) [14]. The ground-state properties of the chemically random U-Zr, Pu-U, and Pu-Zr alloys are obtained from KKR-ASA-CPA

calculations that include the Coulomb screening potential and energy [15-17]. The screening constants are determined from supercell calculations using the locally self-consistent Green's function (LSGF) method [18]. The α and β screening constants, see Refs. [15,16] for details, are found to be 0.70 and 1.06, 0.93 and 1.17, and 0.57 and 0.81, for U-Zr, Pu-U, and Pu-Zr alloys, respectively.

The SR-KKR-ASA-CPA formalism was very successful for describing the ground-state properties of the U-Zr alloys [1], however the present study reveals that relativistic effects are important for Pu-containing systems. Because of this we use the Green's function technique, based on the EMTO formalism, which is not restricted to specific geometries as imposed by the ASA, and also includes the spin-obit coupling through the four-component Dirac equation [19].

The EMTO calculations are performed using both scalar-relativistic and full relativistic Green's function techniques based on the improved screened KKR method, where the one-electron potential is represented by optimized overlapping muffin-tin (OOMT) potential spheres [20, 21]. Inside the potential spheres the potential is spherically symmetric, and it is constant between the spheres. The radii of the potential spheres, the spherical potentials inside the spheres, and the constant value in the interstitial region are determined by minimizing (i) the deviation between the exact and overlapping potentials, and (ii) the errors caused by the overlap between the spheres. Within the EMTO formalism, the one-electron states are calculated exactly for the OOMT potentials. As an output of the EMTO calculations, one can determine self-consistent Green's function of the system and the complete, non-spherically symmetric charged density. Finally, the total energy is calculated using the full charge-density

technique [22]. Like in the case of KKR-ASA calculations, GGA is used for the electron exchange and correlation approximation, and EMTO is combined with the CPA for the calculation of the total energy of chemically random alloys [23]. Integrations over the Brillouin zone and complex energy contour and the choice of the screening constants are identical to those in the KKR-ASA method. Although spin-polarization was not considered in the case of the U-Zr system (non-magnetic solution), the Pu-U and Pu-Zr alloys have been modeled within the disordered local moment approximation that leads to a paramagnetic solution, see Ref. [24] for details.

For the elemental metals, the most accurate and fully relativistic calculations are performed using an all-electron approach where the relativistic effects, including spin-orbit coupling, are accounted for. Although unable to model disorder in the CPA sense it provides important information for the metals, and also serves to confirm the CPA calculations mentioned above. For this purpose we use a version of the FPLMTO [25-27]. The "full potential" in FPLMTO refers to the use of non-spherical contributions to the electron charge density and potential. This is accomplished by expanding the charge density and potential in cubic harmonics inside non-overlapping muffin-tin spheres and in a Fourier series in the interstitial region. We use two energy tails associated with each basis orbital, and for U's semi-core *6s*, *6p* states and valence states (*7s*, *7p*, *6d*, and *5f*) these pairs are different. With this 'double basis' approach we use a total of six energy tail parameters and a total of 12 basis functions per atom. Spherical harmonic expansions are carried out up to l_{max}= 6 for the basis, potential, and charge density. As in the case of the KKR-ASA and EMTO methods, GGA is used for the electron exchange-correlation approximation. A special quasi-random structure (SQS) method, utilizing a 16-atom

supercell, was used to treat the compositional disorder within the FPLMTO formalism [28]. Spin polarization for the Pu-containing alloys was arranged in an antiferromagnetic fashion [29] with neighboring atoms having anti-parallel spins. This is different from the spin configuration used in the EMTO calculations.

3. Ground-state properties of γ-U-Pu-Zr solid solutions

Figure 1a shows results of SR-KKR-ASA-CPA calculations of the heat of formation of the γ-U-Zr solid solutions at T = 0 K [1]. The heat of formation, that shows a positive deviation from the energy associated with a mixture of the pure elements, agrees well with the existence of a miscibility gap in the U-Zr phase diagram. Notice that the calculated heat of formation of the γ-U-Zr solid solutions is in excellent agreement with data derived from a CALPHAD assessment [30] of the experimental thermodynamics and phase diagram information, which validates the *ab initio* approach. For comparison, we also show the heats of formation for the $U_{75}Zr_{25}$, $U_{50}Zr_{50}$, and $U_{25}Zr_{75}$ bcc alloys, calculated within the FPLMTO-SQS technique that agrees pretty well with both SR-KKR-ASA-CPA and CALPHAD assessment results.

Figure 1b show results of SR-KKR-ASA-CPA, SR-EMTO-CPA, and FR-EMTO-CPA calculations of the heat of formation of the γ-Pu-U solid solutions at T = 0 K. Both scalar-relativistic approaches (SR-KKR-ASA and SR-EMTO-CPA) reveal a positive heat of formation that is in a stark contrast with CALPHAD and FPLMTO-SQS results also shown in this Figure. Only when spin-orbit coupling is accounted for within the framework of FR-EMTO-CPA formalism, the calculated heat of formation becomes negative and in excellent agreement with CALPHAD results. In order to understand why

the spin-orbit interaction plays an important role in describing the energetics of Pu-U alloys, we present the calculated equilibrium atomic volumes of bcc Pu and U in the Table. There is a reasonable agreement between the equilibrium atomic volume of bcc U calculated by different approaches. This is not true in the case of bcc Pu, where both KKRASA and SR-EMTO give a significantly larger equilibrium atomic volume than the one calculated within the fully-relativistic approaches (FR-EMTO and FPLMTO). The *f*-band occupation in Pu, calculated within the scalar-relativistic formalisms (SR-KKRASA and SR-EMTO), which is also presented in this Table (in the parenthesis), is about 5.4 that is higher than the 5.1–5.2 calculated when spin-orbit coupling is taken into consideration within the FR-EMTO and FPLMTO methods. The later values are in excellent agreement with the photoelectron spectroscopy estimation [31] as well as recent DMFT results [32]. The present study allows us to conclude that spin-orbit coupling becomes crucially important for calculating the excess thermodynamic characteristics of Pu-containing alloys.

Figure 1c show results of SR-KKR-ASA-CPA, SR-EMTO-CPA, FR-EMTO-CPA, and FPLMTO-SQS calculations for the heat of formation of the γ-Pu-Zr solid solutions at T = 0 K. All CPA-related models reveal a change in the sign of the heat of formation as a function of alloy composition with a tendency towards phase formation for Zr-rich alloys. However this energetic evolution is in contrast with the CALPHAD results. One plausible explanation is that the CALPHAD results were obtained from data for the high-temperature part of the Pu-Zr phase diagram. Therefore it is likely that the γ-phase is primarily stabilized by entropy. It is also worth noting that in all cases the extremum heat of formation is small (note the energy scale compared to the one for U-Zr

or U-Pu case), hence reinforcing the assumption that the bcc phase is mainly stabilized by entropy at high temperatures. Comparing results of the EMTO calculations reveals that spin-orbit interaction has also a significant effect in the Pu-Zr system, although not as strong as it is appears for U-Pu alloys. We believe that a fully-relativistic treatment is necessary for an accurate determination of the energetics of all Pu-based alloys.

Figure 2 shows results of calculations of the equilibrium atomic volume of the bcc U-Zr, Pu-Zr, and Pu-U alloys at $T = 0$ K. There is a positive deviation from Vegard's law for the γ-U-Zr alloys (results of SR-KKRASA-CPA calculations) that is in accord with the positive heat of formation in this system. Results of FR-EMTO-CPA calculations for Pu-Zr and Pu-U alloys, shown in this Figure, indicate a negative deviation from Vegard's law for the equilibrium atomic volume of the γ-Pu-U alloys that agrees well with the negative formation energy of these alloys. The sign change in the Vegard's law deviation in the γ-Pu-Zr system correlates well with the composition dependence of the formation energy of these alloys.

4. Conclusion

In the present paper *ab initio* results are obtained for the U-Pu-Zr alloys to understand the effectiveness of first-principles methods in describing actinide alloys. Ground-state properties of the bcc U-Z, Pu-U, and Pu-Zr solid solutions were calculated. These *ab initio* results will be used to build a thermodynamic database with important input from *ab initio* that will be directly comparable to the results obtained solely from experimental data on thermodynamic properties and phase diagram. On one hand, as was mentioned in Refs. [3,33], fuel-cladding interdiffusion could be significantly enhanced by

lanthanides fission products that are present in increasing amount with higher burnup that could lead to regions with lower melting temperatures in the fuel, effectively thinning the cladding. On the other hand, the main goal of fast spectrum breeder reactors is to achieve high burn-up by fissioning all types of transuranic elements with complete transmutation of long-lived minor actinides, with the result of creating a closed nuclear fuel cycle with future disposition of the nuclear fuel waste products in a single geological repository [34]. Our combined *ab initio* and CALPHAD approach will serve as a template to investigate a mixture of U and Pu with lanthanide fusion products, La, Ce, Pr, Ne, and Sm, and long-lived minor actinides, Np, Am, and Cu, for which experimental data are lacking. That is why the improved and validated coupling between *ab initio* and CALPHAD methodologies, that we plan to accomplish, will allow us to predict the thermodynamic driving force, associated with any actinide-based alloys, and this will be used as an input for predicting microstructure evolution and site redistribution, and help to validate the development of phenomenological interatomic potentials for subsequent molecular dynamics simulations.

Acknowledgements

This work was performed under the auspices of the U.S. Department of Energy by Lawrence Livermore National Laboratory under contract DE-AC52-07NA27344.

References:

1. A. Landa, P. Söderlind, P.E.A. Turchi, L. Vitos, A. Ruban, J. Nucl. Mater. (2008), doi:10.1016/j.jnucmat.2008.09.029.

2. G.L. Hofman, S.L. Hayes, M.C. Petri, J. Nucl. Mater. 227 (1996) 277-286.
3. G.L. Hofman, L.C. Walters, T.H. Bauer, Progr. Nucl. Energy 31 № 1/2 (1997) 83-110.
4. Y.H. Sohn, M.A. Dayananda, G.L. Hofman, R.V. Strain, S.L. Hayes, J. Nucl. Mater. 279 (2000) 317-329.
5. Yeon Soo Kim, G.L. Hofman, S.L. Hayes, Y.H Sohn, J. Nucl. Mater. 327 (2004) 27-36.
6. Yeon Soo Kim, S.L. Hayes, G.L. Hofman, A.M. Yacout, J. Nucl. Mater. 359 (2006) 17-28.
7. O. Gunnarson, O. Jepsen, O.K. Andersen, Phys. Rev B 27 (1983) 7144-7168.
8. I.A. Abrikosov, H.L. Skriver, Phys. Rev B 47 (1993) 16532-16541.
9. A.V. Ruban, H.L. Skriver, Comput. Mater. Sci. 15 (1999) 119-143.
10. N.E. Christensen, S. Satpathy, Phys. Rev. Lett. 55 (1985) 600-603.
11. J.P. Perdew, K. Burke, M. Ernzerhof, Phys. Rev. Lett. 77 (1996) 3865-3868.
12. D.J. Chadi, M.L. Cohen, Phys. Rev. B 8 (1973) 5747-5753; Phys. Rev B 39 (1989) 3168-3172.
13. F.D. Murnaghan, Proc. Natl. Acad. Sci. U.S.A. 30 (1944) 244-247.
14. J.S. Faulkner, Prog. Mater. Sci. 27 (1982) 1-187.
15. A.V. Ruban, H.L. Skriver, Phys. Rev. B 66 (2002) 024201-1-15.
16. A.V. Ruban, S.I. Simak, P.A. Korzhavyi, H.L. Skriver, Phys. Rev. B 66 (2002) 024202-1-12.
17. A.V. Ruban, S.I. Simak, S. Shallcross, H.L. Skriver, Phys. Rev. B 67 (2003) 214302-1-12.

18. I.A. Abrikosov, S.I. Simak, B. Johansson, A.V. Ruban, H.L. Skriver, Phys. Rev. B 56 (1997) 9319-9334.
19. L. V. Pourovskii, A. V. Ruban, L. Vitos, H. Ebert, B. Johansson, I. A. Abrikosov, Phys. Rev. B 71 (2005) 094415-1-10.
20. L. Vitos, Phys. Rev B 64 (2001) 014107-1-11.
21. L. Vitos, Computational Quantum Mechanics for Materials Engineers: The EMTO Method and Application, Springer, London, 2007.
22. J. Kollar, L. Vitos, H.L. Skriver, in: H. Dreyssé (Ed.), Electronic Structure and Physical Properties of Solids: The Uses of the LMTO Method, Lecture Notes in Physics, Springer, Berlin, 2000, pp. 85-113.
23. L. Vitos, I.A. Abrikosov, B. Johansson, Phys. Rev. Lett. 87 (2001) 156401-4.
24. P. Söderlind, A. Landa, B. Sadigh, Phys. Rev. B 66 (2002) 205109-1-6; A. Landa, P. Söderlind, J. Alloys Comp. 354 (2003) 99-103.
25. J.M. Wills, B. Cooper, Phys. Rev. B 36 (1987) 3809-3823.
26. D.L. Price, B. Cooper, Phys. Rev. B 39 (1989) 4945-4957.
27. J.M. Wills, O. Eriksson, M. Alouani, D.L. Price, in: H. Dreyssé (Ed.), Electronic Structure and Physical Properties of Solids: The Uses of the LMTO Method, Lecture Notes in Physics, Springer, Berlin, 2000, pp.148-167.
28. A. Zunger, S.H. Wei, L.G. Ferreira, J.E. Bernard, Phys. Rev. Lett. 65 (1990) 353-356.
29. P. Söderlind, B. Sadigh, Phys. Rev. Lett. 92 (2004) 185702-1-4.

30. P.E.A. Turchi, I.A. Abrikosov, B. Burton, S.G. Fries, G. Grimvall, L. Kauffman, P. Korzhavyi, V. Rao Manga, M. Ohno, A. Pisch, A. Scott, W. Zhang, CALPHAD 31 (2007) 4-27.
31. J.G. Tobin, P. Söderlind, A. Landa, K.T. Moore, A.J. Schwartz, B.W. Chung, M.A. Wall, J. M. Wills, R.G. Haire, A.L. Kutepov, J. Phys.: Condens. Matter 20 (2008) 125204-1-9.
32. J.H. Shim, K. Haule, G. Kotliar, Nature 446 (2007) 513-516.
33. J. D. Petti, D. Crawford, N. Chauvin, MRS Bulletin 34 № 1 (2009) 40-45.
34. D.D Keiser Jr., J.B. Kennedy, B.A. Hilton, S.L. Hayes, JOM № 1 (2008) 29-32.

Table

Equilibrium atomic volume (in $Å^3$) of bcc Pu, U, and Zr. *f*- and *d*-band occupations are shown in parentheses for actinides (Pu and U) and Zr, respectively.

Metal	KKR-ASA	SR-EMTO	FR-EMTO	FPLMTO
Pu	27.82 (5.36)	26.14 (5.40)	24.05 (5.24)	23.30 (5.11)
U	21.08 (2.91)	20.96 (2.98)	21.25 (2.89)	20.41 (2.75)
Zr	23.46 (2.65)	22.93 (2.70)	22.93 (2.70)	22.76 (2.40)

Captions

Figure 1. Heat of formation (in mRy/atom) versus composition for γ-U-Zr (a), γ-Pu-U (b), and γ-Pu-Zr (c) alloys (T = 0 K).

Figure 2. Atomic volume (in $Å^3$) versus composition for γ-U-Zr (a), γ-Pu-U (b), and γ-Pu-Zr (c) alloys (T = 0 K). U-Zr – KKR-ASA-CPA, Pu-U and Pu-Zr – FR-EMTO-CPA.

Figures.

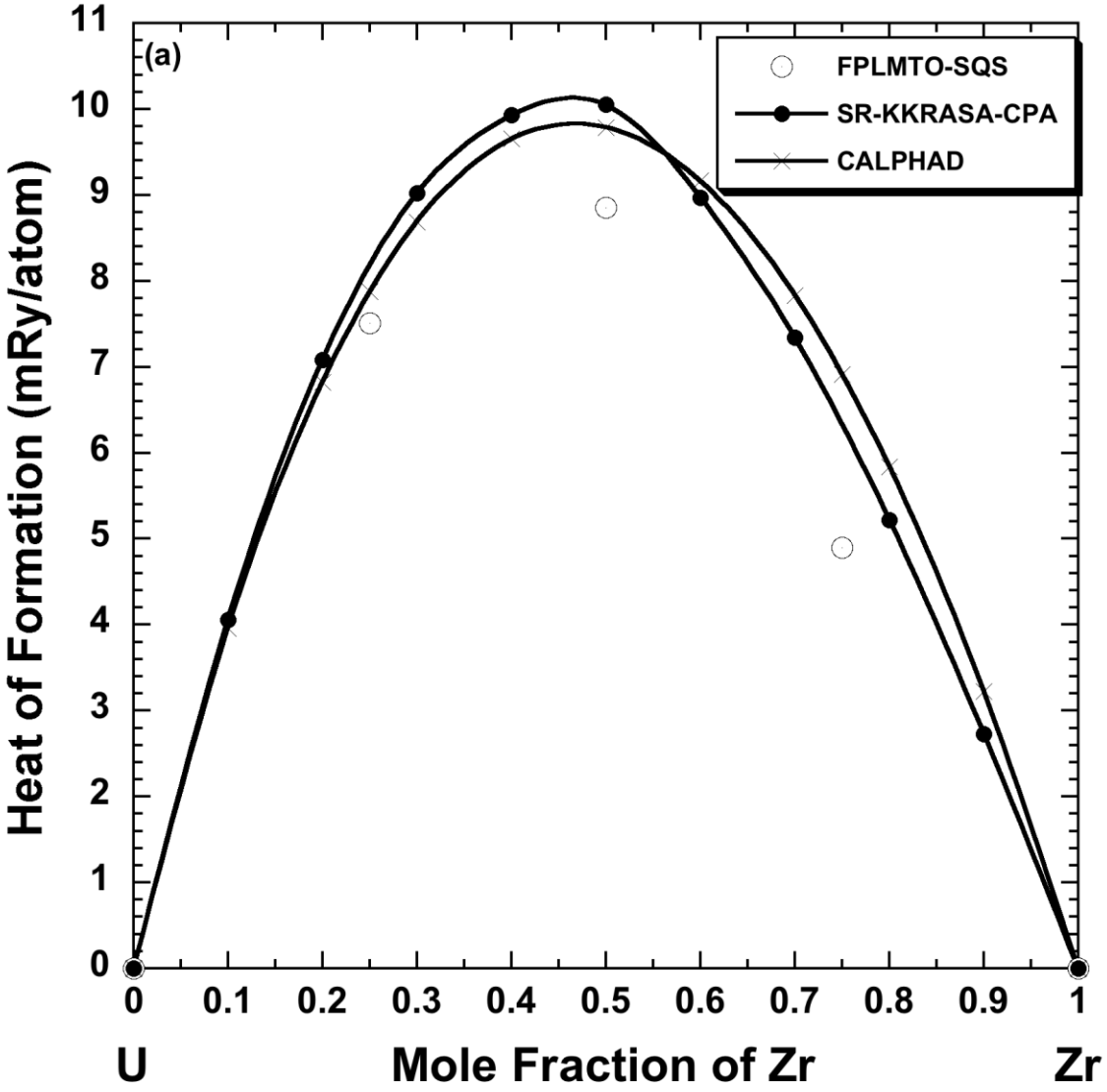

Figure 1a.

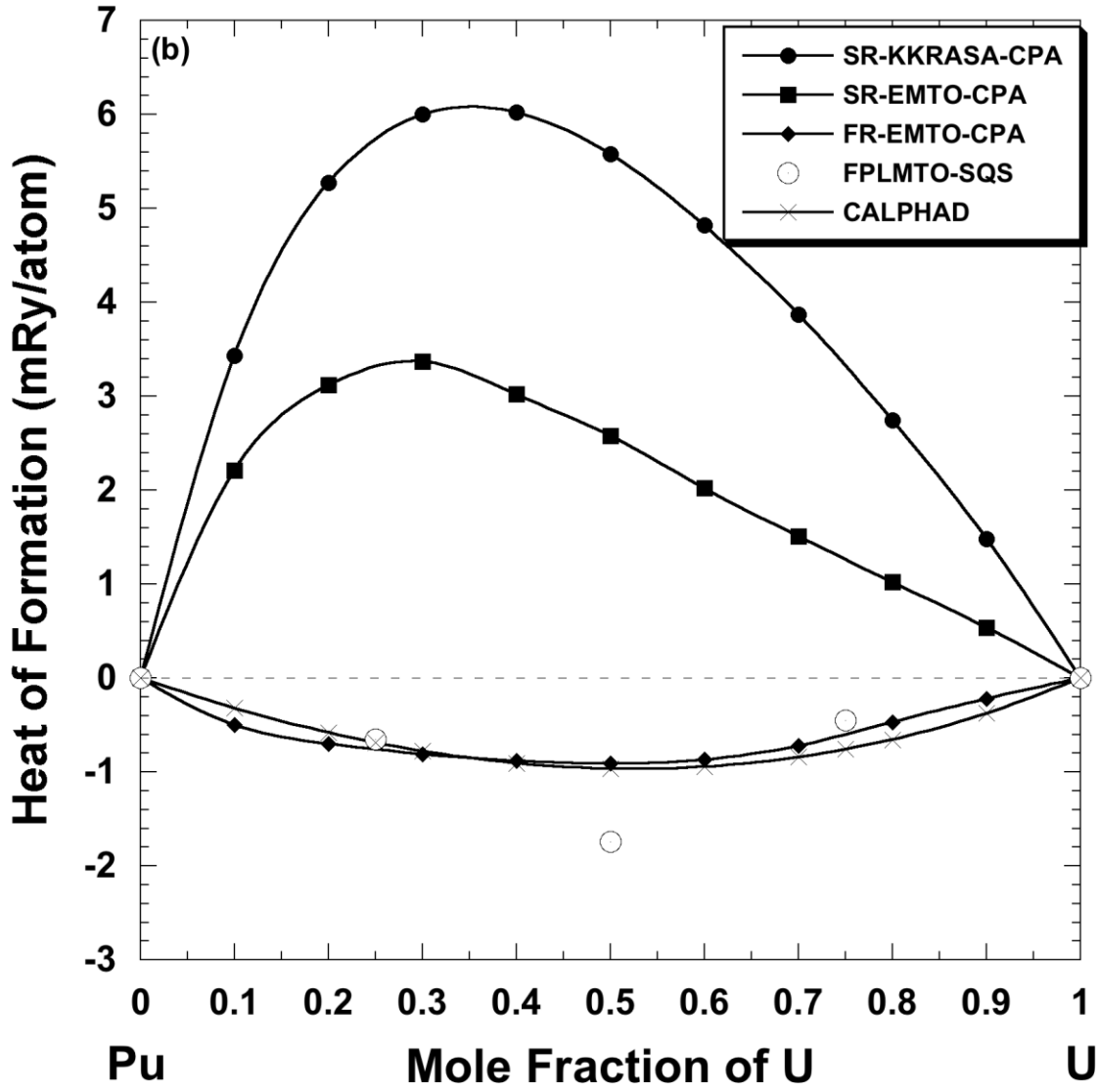
(b)
SR-KKRASA-CPA
SR-EMTO-CPA
FR-EMTO-CPA
FPLMTO-SQS
CALPHAD
Heat of Formation (mRy/atom)
7
6
5
4
3
2
1
0
-1
-2
-3
0
0.1
0.2
0.3
0.4
0.5
0.6
0.7
0.8
0.9
1
Pu
Mole Fraction of U
U

Figure 1b.

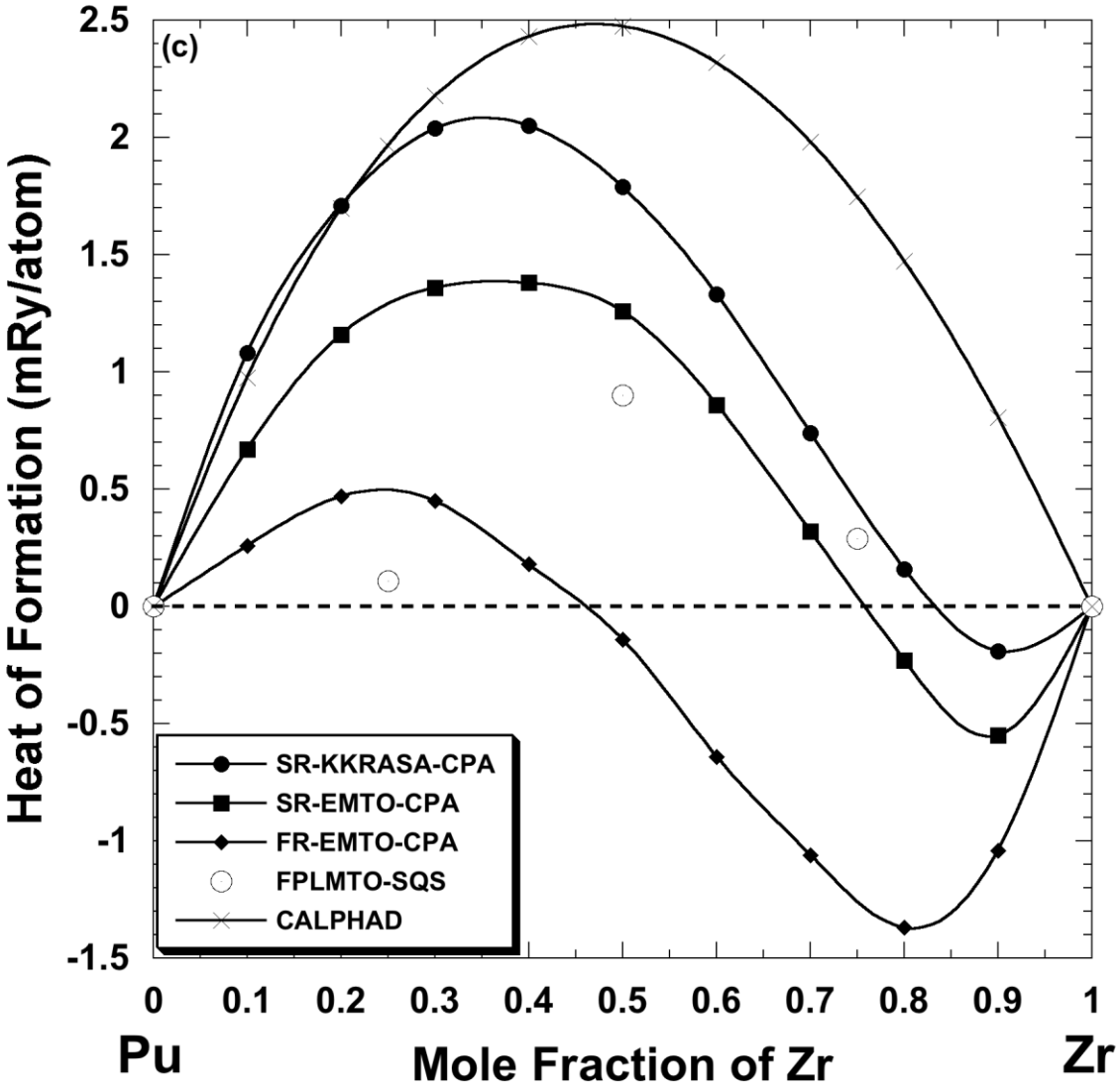
(c)
Heat of Formation (mRy/atom)
2.5
2
1.5
1
0.5
0
-0.5
-1
-1.5
0
0.1
0.2
0.3
0.4
0.5
0.6
0.7
0.8
0.9
1
Pu
Mole Fraction of Zr
Zr
SR-KKRASA-CPA
SR-EMTO-CPA
FR-EMTO-CPA
FPLMTO-SQS
CALPHAD

Figure 1c.

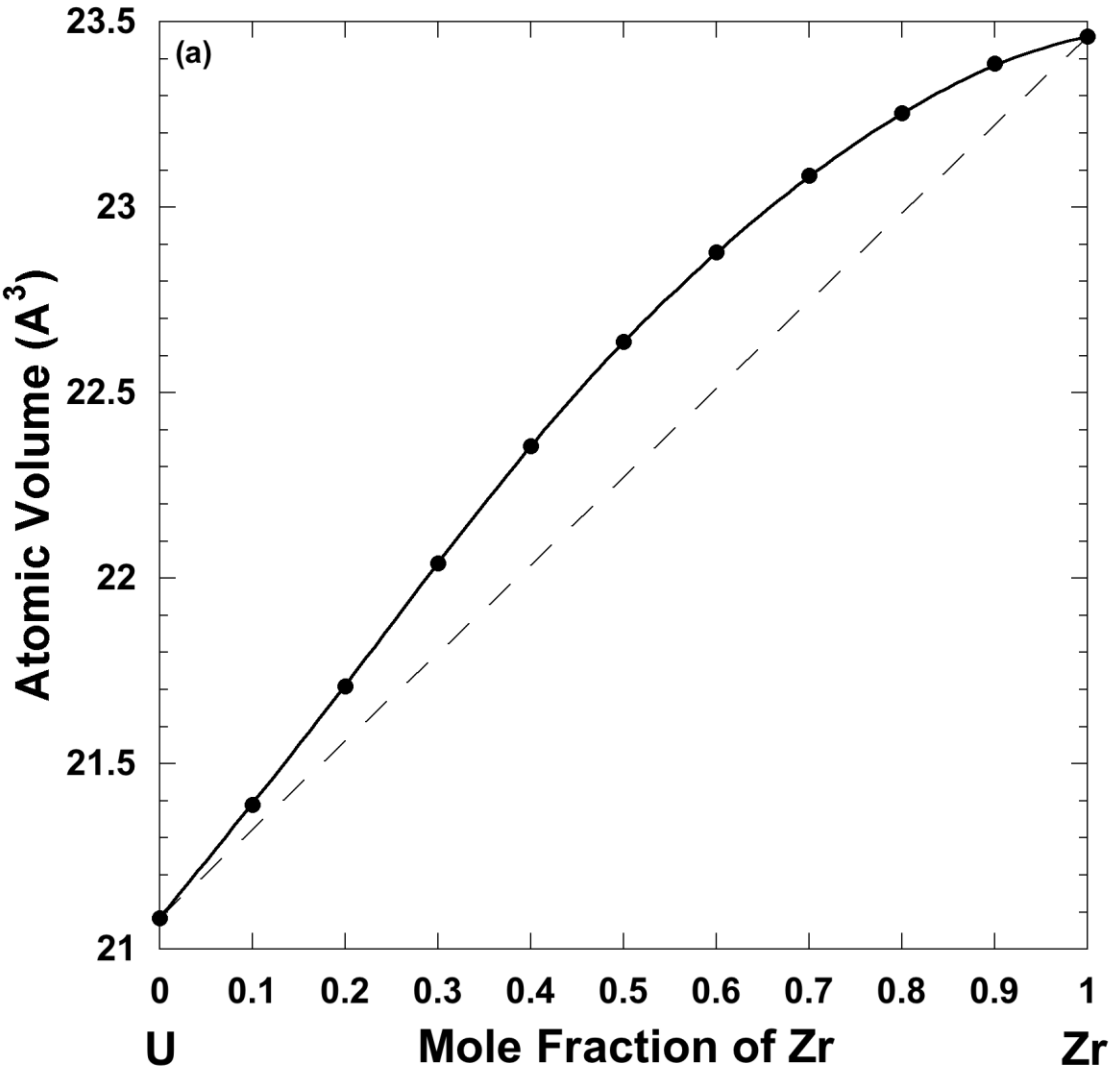
(a)
Atomic Volume (A^3)
23.5
23
22.5
22
21.5
21
0
0.1
0.2
0.3
0.4
0.5
0.6
0.7
0.8
0.9
1
U
Mole Fraction of Zr
Zr

Figure 2a.

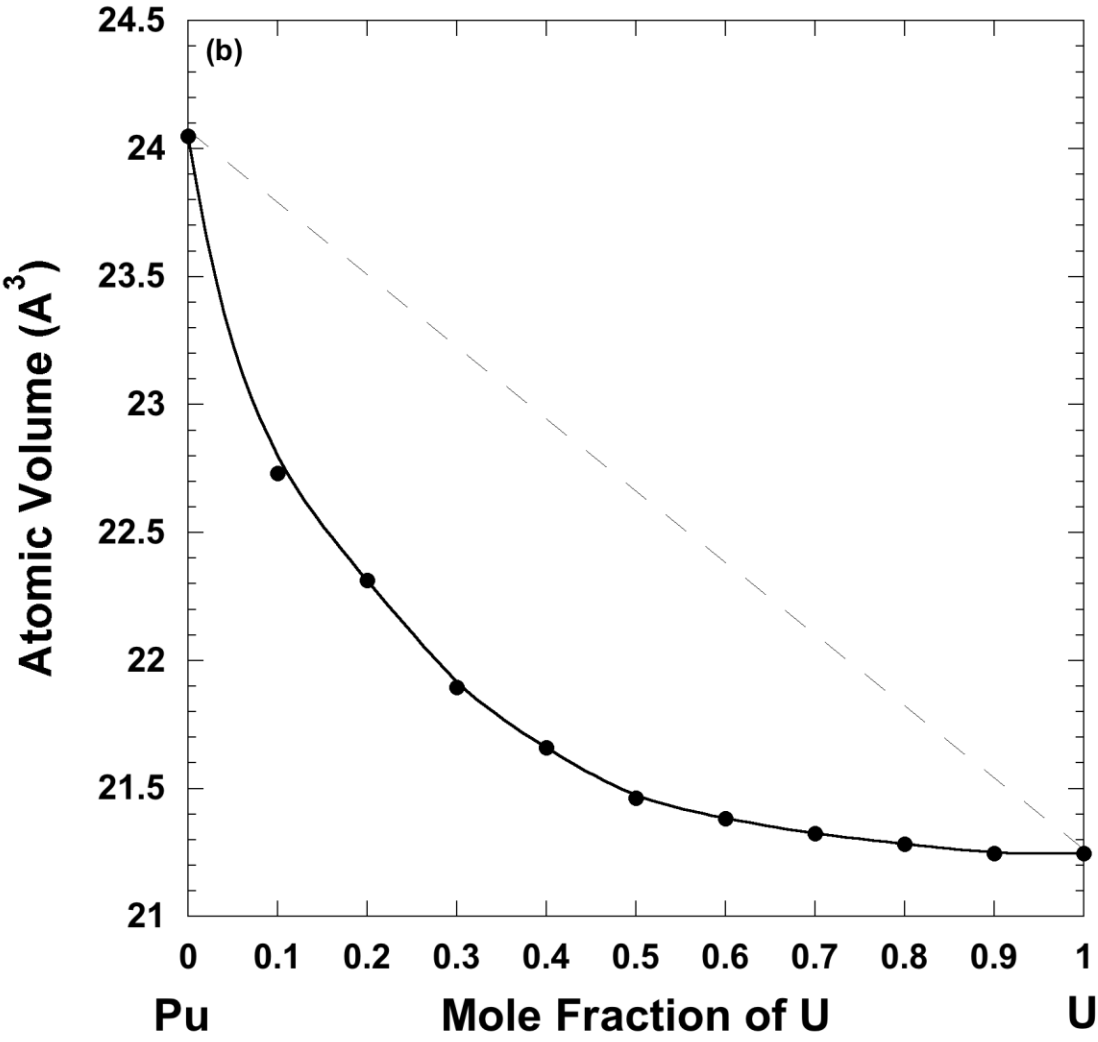
(b)
Atomic Volume (A^3)
24.5
24
23.5
23
22.5
22
21.5
21
0
0.1
0.2
0.3
0.4
0.5
0.6
0.7
0.8
0.9
1
Pu
Mole Fraction of U
U

Figure 2b.

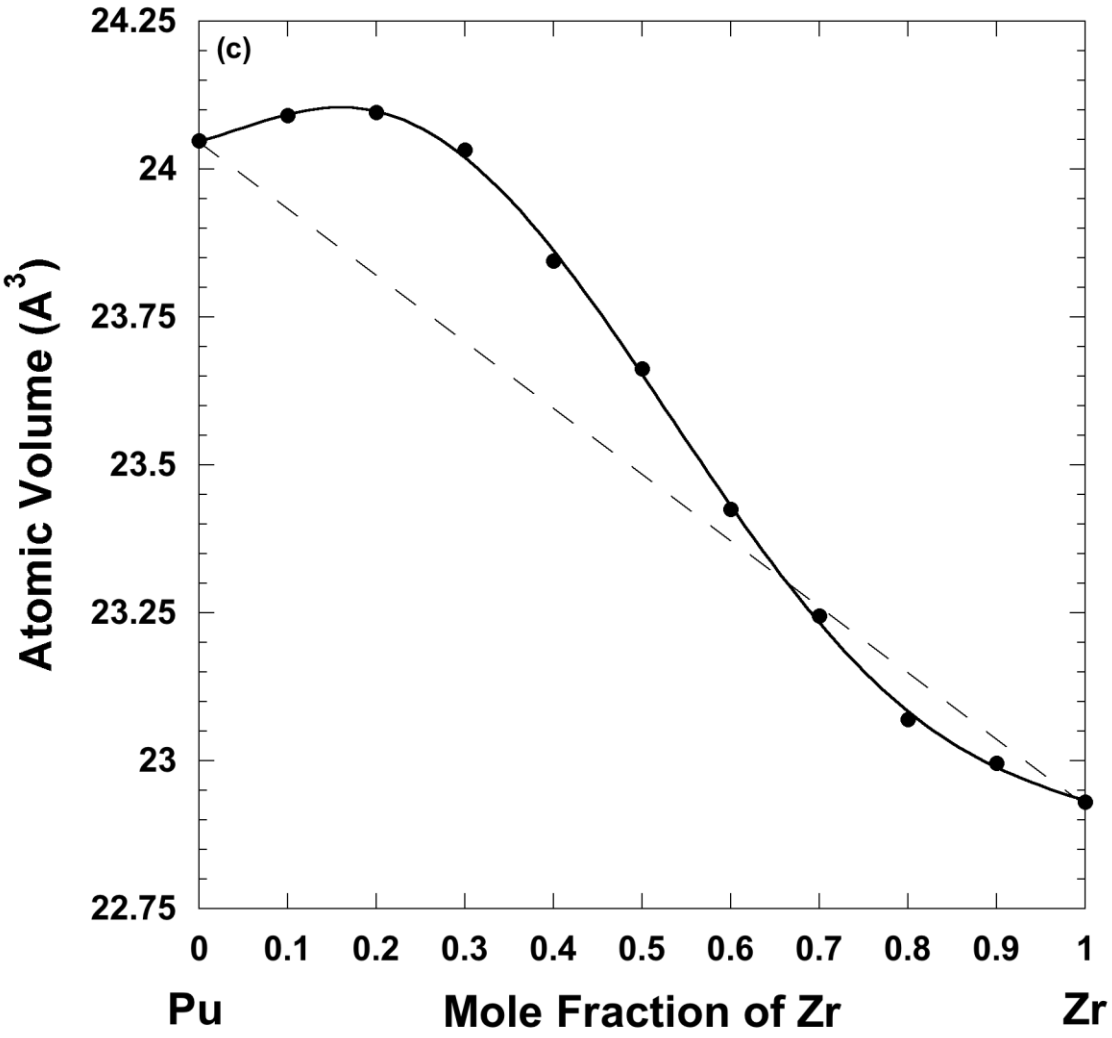
(c)
24.25
24
23.75
23.5
23.25
23
22.75
Atomic Volume (A^3)
0
0.1
0.2
0.3
0.4
0.5
0.6
0.7
0.8
0.9
1
Pu
Mole Fraction of Zr
Zr

Figure 2c.